ANNUAL REVIEWS

Annual Review of Earth and Planetary Sciences

Global Patterns of Carbon Dioxide Variability from Satellite Observations

Xun Jiang[1] and Yuk L. Yung[2,3]

[1]Department of Earth and Atmospheric Sciences, University of Houston, Houston, Texas 77204, USA; email: xjiang7@uh.edu

[2]Division of Geological and Planetary Sciences, California Institute of Technology, Pasadena, California 91125, USA; email: yly@gps.caltech.edu

[3]Jet Propulsion Laboratory, Pasadena, California 91109, USA

Annu. Rev. Earth Planet. Sci. 2019. 47:225–45

First published as a Review in Advance on January 11, 2019

The *Annual Review of Earth and Planetary Sciences* is online at earth.annualreviews.org

https://doi.org/10.1146/annurev-earth-053018-060447

Keywords

CO_2 annual cycle, CO_2 semiannual cycle, intraseasonal variability, monsoon, El Niño–Southern Oscillation, Northern Annular Mode, drought, wildfire

Abstract

Advanced satellite technology has been providing unique observations of global carbon dioxide (CO_2) concentrations. These observations have revealed important CO_2 variability at different timescales and over regional and planetary scales. Satellite CO_2 retrievals have revealed that stratospheric sudden warming and the Madden-Julian Oscillation can modulate atmospheric CO_2 concentrations in the mid-troposphere. Atmospheric CO_2 also demonstrates variability at interannual timescales. In the tropical region, the El Niño–Southern Oscillation and the Tropospheric Biennial Oscillation can change atmospheric CO_2 concentrations. At high latitudes, mid-tropospheric CO_2 concentrations can be influenced by the Northern Hemispheric annular mode. In addition to modulations by the large-scale circulations, sporadic events such as wildfires, volcanic eruptions, and droughts, which change CO_2 surface emissions, can cause atmospheric CO_2 concentrations to increase significantly. The natural variability of CO_2 summarized in this review can help us better understand its sources and sinks and its redistribution by atmospheric motion.

- Global satellite CO_2 data offer a unique opportunity to explore CO_2 variability in different regions.

- Atmospheric CO_2 concentration demonstrates variations at intraseasonal, seasonal, and interannual timescales.
- Both large-scale circulations and variations of surface emissions can modulate CO_2 concentrations in the atmosphere.

1. INTRODUCTION

Atmospheric carbon dioxide (CO_2) is an important greenhouse gas and has a big impact on the radiative budget (e.g., Goody & Yung 1989, IPCC 2013). As shown in **Figure 1**, the major absorption bands of CO_2 are at 540–800 cm^{-1}, 850–1,250 cm^{-1}, and 2,100–2,400 cm^{-1} (Goody & Yung 1989), where they trap infrared radiation emitted from the Earth and warm the atmosphere and surface. The concentration of atmospheric CO_2 is increasing with a positive trend of ~2 ppm/year (e.g., Keeling et al. 1995, Sarmiento & Wofsy 1999, Tans & Keeling 2014), which has a significant influence on global warming (e.g., Dickinson & Cicerone 1986, IPCC 2013). To understand its variations, researchers have used different data sets to monitor atmospheric CO_2 concentration. Surface, aircraft, and satellite CO_2 data are summarized in **Table 1**. The National Oceanic and Atmospheric Administration Earth System Research Laboratory (NOAA ESRL) network has ~155 CO_2 measurement stations monitoring atmospheric CO_2 at the surface (Tans et al. 1998, GLOBALVIEW-CO2 2010). The Total Carbon Column Observing Network (TCCON) has ~20 surface stations that use a ground-based Fourier transform spectrometer to measure column CO_2 (Washenfelder et al. 2006, Wunch et al. 2011). In addition to the surface measurements, there are also aircraft CO_2 data, such as those from NOAA ESRL (GLOBALVIEW-CO2 2010), Comprehensive Observation Network for TRace gases by AIrLiner (CONTRAIL) (Matsueda et al. 2002), Intercontinental Chemical Transport Experiment-North America (INTEX-NA) (Singh et al. 2002, Choi et al. 2008), HIAPER Pole-to-Pole (HIPPO) (Wofsy 2011), In-service Aircraft

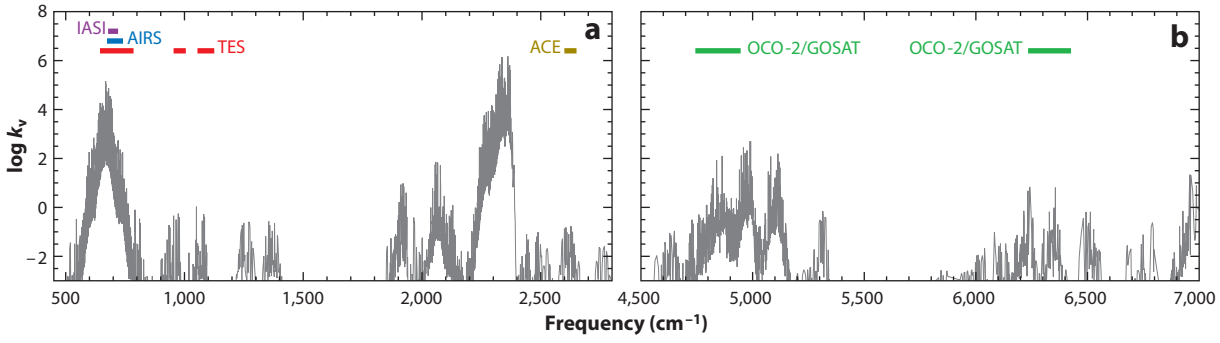

Figure 1

CO_2 absorption coefficients derived from the high-resolution transmission molecular absorption database. The lines shown indicate channels used to retrieve CO_2 from the OCO-2 and GOSAT (*green*), TES (*red*), AIRS (*blue*), IASI (*purple*), and ACE (*dark yellow*). Abbreviations: ACE, Atmospheric Chemistry Experiment; AIRS, Atmospheric Infrared Sounder; CO_2, carbon dioxide; GOSAT, Greenhouse gases Observing SATellite; IASI, Infrared Atmospheric Sounding Interferometer; OCO-2, Orbiting Carbon Observatory 2; TES, Tropospheric Emission Spectrometer.

Table 1 Summary of surface, aircraft, and satellite CO_2 data sets

Type	Data	CO_2 channels (cm^{-1})
Surface CO_2	NOAA ESRL surface CO_2	NA
	TCCON column CO_2	NA
Aircraft CO_2	NOAA ESRL aircraft CO_2	NA
	CONTRAIL aircraft CO_2	NA
	INTEX-NA aircraft CO_2	NA
	HIPPO aircraft CO_2	NA
	IAGOS aircraft CO_2	NA
	CARVE aircraft CO_2	NA
Satellite CO_2	OCO-2 column CO_2 (X_{CO2})	6,250–6,410, 4,760–4,930
	GOSAT column CO_2 (X_{CO2})	6,250–6,410, 4,760–4,930
	TES mid-tropospheric CO_2	660–770, 970–990, 1,070–1,110
	AIRS mid-tropospheric CO_2	690–725
	IASI mid-tropospheric CO_2	694–705
	ACE mid-tropospheric CO_2	2,615–2,635

CO_2 channels used to retrieve satellite CO_2 are also listed. Abbreviations: ACE, Atmospheric Chemistry Experiment; AIRS, Atmospheric Infrared Sounder; CARVE, Carbon in Arctic Reservoirs Vulnerability Experiment; CO_2, carbon dioxide; CONTRAIL, Comprehensive Observation Network for Trace gases by AIrLiner; HIPPO, HIAPER Pole-to-Pole; GOSAT, Greenhouse gases Observing SATellite; IAGOS, In-service Aircraft for a Global Observing System; IASI, Infrared Atmospheric Sounding Interferometer; INTEX-NA, Intercontinental Chemical Transport Experiment-North America; NA, not applicable; NOAA ESRL, National Oceanic and Atmospheric Administration Earth System Research Laboratory; OCO-2, Orbiting Carbon Observatory 2; TCCON, Total Carbon Column Observing Network; TES, Tropospheric Emission Spectrometer.

for a Global Observing System (IAGOS) (Petzold et al. 2015), and Carbon in Arctic Reservoirs Vulnerability Experiment (CARVE) (Dupont et al. 2012, Fisher et al. 2014).

Previous in situ CO_2 measurements at the surface or from aircraft are limited in spatial extent, so it is difficult to explore CO_2 variability over the global domain. In recent years, satellite missions have provided global measurements of atmospheric CO_2 concentration (e.g., Barkley et al. 2006; Chahine et al. 2008; Strow & Hannon 2008; Crevoisier et al. 2009; Yokota et al. 2009; Kulawik et al. 2010; Rinsland et al. 2010; Boesch et al. 2011; Foucher et al. 2011; Crisp et al. 2012, 2017; Nguyen et al. 2014; Eldering et al. 2017). Absorption bands for retrieving CO_2 concentration from different satellites are shown in **Figure 1**. The weak CO_2 absorption band at 6,250–6,410 cm^{-1} (1.58 μm) is combined with the absorption band at 4,760–4,930 cm^{-1} (2.06 μm) to retrieve CO_2 abundances from the Orbiting Carbon Observatory 2 (OCO-2) satellite (Kuang et al. 2002) and Greenhouse gases Observing SATellite (GOSAT) (Shiomi et al. 2008, Watanabe et al. 2008, Kuze et al. 2009). CO_2 channels at 660–770 cm^{-1}, 970–990 cm^{-1}, and 1,070–1,110 cm^{-1} are used to retrieve mid-tropospheric CO_2 from the Tropospheric Emission Spectrometer (TES) (Kulawik et al. 2010). Absorption bands at 690–725 cm^{-1}, 694–705 cm^{-1}, and 2,615–2,635 cm^{-1} are used to derive mid-tropospheric CO_2 from the Atmospheric Infrared Sounder (AIRS) (Chahine et al. 2008), Infrared Atmospheric Sounding Interferometer (IASI) (Crevoisier et al. 2009), and Atmospheric Chemistry Experiment (ACE) (Rinsland et al. 2010), respectively. These globally distributed CO_2 retrievals from satellites offer a unique opportunity to explore atmospheric CO_2 variability over the planetary scale.

Surface, aircraft, and satellite data provide CO_2 information at different altitudes. For example, data from NOAA ESRL provide CO_2 measurements at the surface. However, they are limited in

spatial extent and do not contain CO_2 vertical profiles. Aircraft CO_2 data (e.g., NOAA ESRL, CONTRAIL, INTEX-NA, HIPPO, IAGOS, CARVE) provide additional information on CO_2 vertical structure, but they are limited in spatial extent and are not continuous. Recent satellite CO_2 retrievals provide continuous global maps of column CO_2 (e.g., OCO-2 and GOSAT) and mid-tropospheric CO_2 (e.g., ACE, AIRS, IASI, and TES). In this article, we discuss the variability of atmospheric CO_2 concentrations, especially new results emerging from satellite data.

2. IMPACTS OF BIOSPHERE AND LARGE-SCALE ATMOSPHERIC CIRCULATION ON CO_2 CONCENTRATIONS

2.1. Annual and Semiannual Cycles of CO_2

Atmospheric CO_2 concentration demonstrates an annual cycle. Using in situ CO_2 measurements, previous studies (Pearman & Hyson 1980, 1981; Cleveland et al. 1983; Bacastow et al. 1985; Keeling et al. 1996; Shia et al. 2006; Buermann et al. 2007) explored the CO_2 annual cycle over different locations and revealed that it is related to the interaction between the biosphere and the atmosphere. Recent satellite retrievals provide CO_2 data over the global domain and offer a unique opportunity to explore the CO_2 annual cycle over different regions (e.g., Chahine et al. 2005, Crevoisier et al. 2009, Kulawik et al. 2010, Rinsland et al. 2010, Lindqvist et al. 2015, Jiang et al. 2016, Eldering et al. 2017). Using CO_2 retrievals from the IASI, Crevoisier et al. (2009) revealed a larger CO_2 annual cycle in the Northern Hemisphere than in the Southern Hemisphere for the upper tropospheric (11–15 km). Chahine et al. (2005) compared mid-tropospheric CO_2 from AIRS with CONTRAIL CO_2 aircraft data and found that the satellite-derived AIRS mid-tropospheric CO_2 captures the correct CO_2 annual cycle in both hemispheres. Kulawik et al. (2010) compared mid-tropospheric CO_2 from TES to CO_2 data from Mauna Loa, CarbonTracker, and CONTRAIL data and found a consistent CO_2 annual cycle among different data sets. Rinsland et al. (2010) analyzed satellite-derived ACE mid-tropospheric CO_2 retrievals and found a CO_2 annual cycle similar to the GLOBALVIEW aircraft CO_2 data. The GOSAT column CO_2 measurements were compared to the ground-based TCCON data and were found to have similar CO_2 annual cycles (Lindqvist et al. 2015). Eldering et al. (2017) calculated weekly averaged OCO-2 column CO_2 data from Hawaii, EuroAsia, and the South Pacific. As shown in **Figure 2**, OCO-2 column CO_2 annual cycle amplitudes are larger in Hawaii and EuroAsia than in the South Pacific because there is less CO_2 surface emission and uptake in the South Pacific (Eldering et al. 2017). In addition to the annual cycle, atmospheric CO_2 also demonstrates a semiannual cycle, which is related to the biosphere-atmosphere exchange (Jiang et al. 2012).

Using a multiple regression method, Jiang et al. (2016) studied CO_2 annual cycle and semiannual cycle amplitudes from different satellite CO_2 retrievals (e.g., GOSAT, AIRS, TES), NOAA ESRL surface CO_2, and TCCON column CO_2. As shown in **Figure 3**, of all these data sets, NOAA ESRL surface CO_2 has the largest annual cycle and semiannual cycle amplitudes; AIRS mid-tropospheric CO_2 has the smallest annual cycle and semiannual cycle amplitudes. Annual cycle and semiannual cycle amplitudes derived from GOSAT X_{CO2} (column-averaged CO_2 dry air mole fraction) are consistent with those from TCCON X_{CO2} but smaller than those in the NOAA ESRL surface data. All CO_2 data correctly demonstrate the latitudinal gradient for CO_2 annual cycle amplitudes, with larger amplitudes in the Northern Hemisphere than the Southern Hemisphere. **Figure 3** also demonstrates that the amplitudes of CO_2 annual and semiannual cycles decrease with altitude (Jiang et al. 2016) because the sources of cycles are located at the surface and the signals decay with the altitude. The Model for OZone And Related chemical Tracers-2 (MOZART-2) and CarbonTracker models were used to explore the CO_2 annual cycle. The CO_2

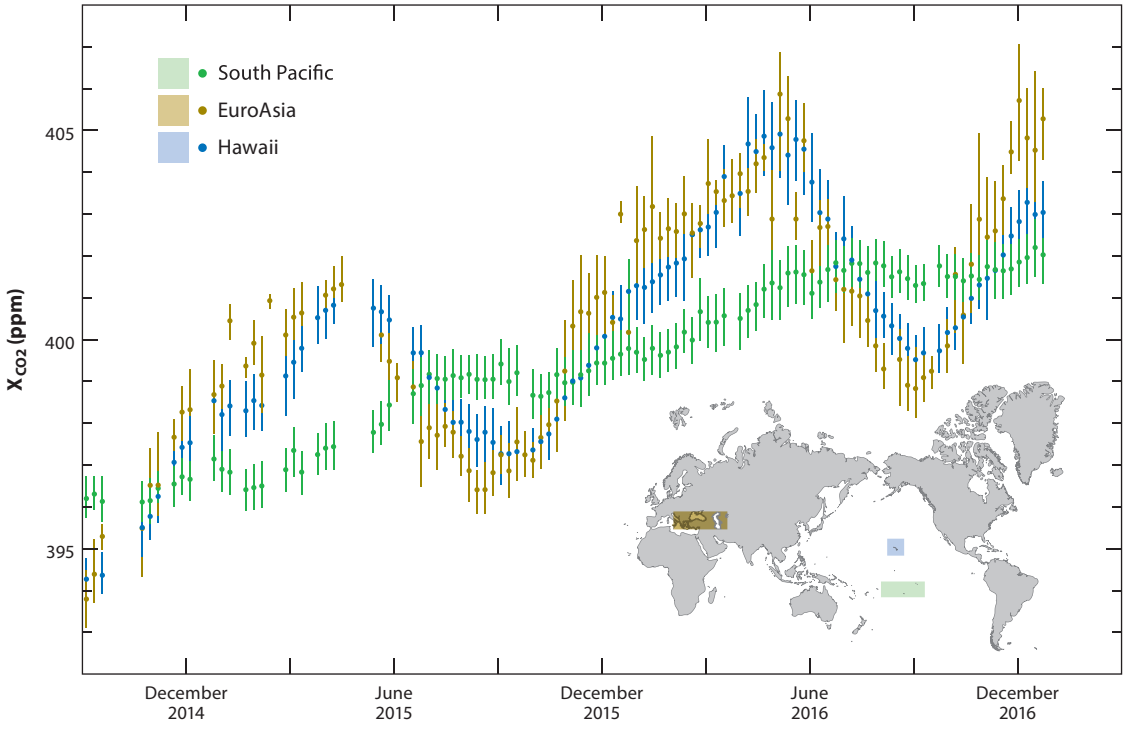

Figure 2

OCO-2 CO_2 data from Hawaii (*blue*), EuroAsia (*dark yellow*), and the South Pacific (*green*). X_{CO2} is the CO_2 dry air mole fraction in units of parts per million. Abbreviations: CO_2, carbon dioxide; OCO-2, Orbiting Carbon Observatory 2. Figure adapted from Eldering et al. (2017) with permission from AAAS.

annual cycle results from these models are similar to those from the satellite CO_2 retrievals in most regions except the Northern Hemisphere mid-latitudes, which might be related to the weak convective mass flux (Jiang et al. 2008) and underestimation of net ecosystem exchange in the models (Yang et al. 2007). These results can help us to better understand the vertical distribution of atmospheric CO_2 and identify possible deficiencies in the models.

2.2. Intraseasonal Variability of CO_2

In addition to the annual cycle and semiannual cycle, atmospheric CO_2 also demonstrates intraseasonal variability.

2.2.1. Influence of the Madden-Julian Oscillation. Intraseasonal variability, such as the Madden-Julian Oscillation (MJO), can modulate mid-troposphere CO_2 concentrations in the tropics and polar region (Li et al. 2010, Li 2018). MJO is an important intraseasonal feature with a period of about 30–90 days (Madden & Julian 1971). It can influence convection, rainfall, winds, and chemical tracers (Knutson & Weickmann 1987, Tian et al. 2007, Jiang et al. 2009). **Figure 4** demonstrates the MJO-related mid-tropospheric CO_2 anomalies and the Tropical Rainfall Measuring Mission rainfall anomalies for eight phases of the MJO. The eight MJO phases are defined by the All-season Real-time Multivariate MJO index and represent different phases of the MJO cycle in a temporal sequence, as MJO propagates from the Indian Ocean to the eastern Pacific. The

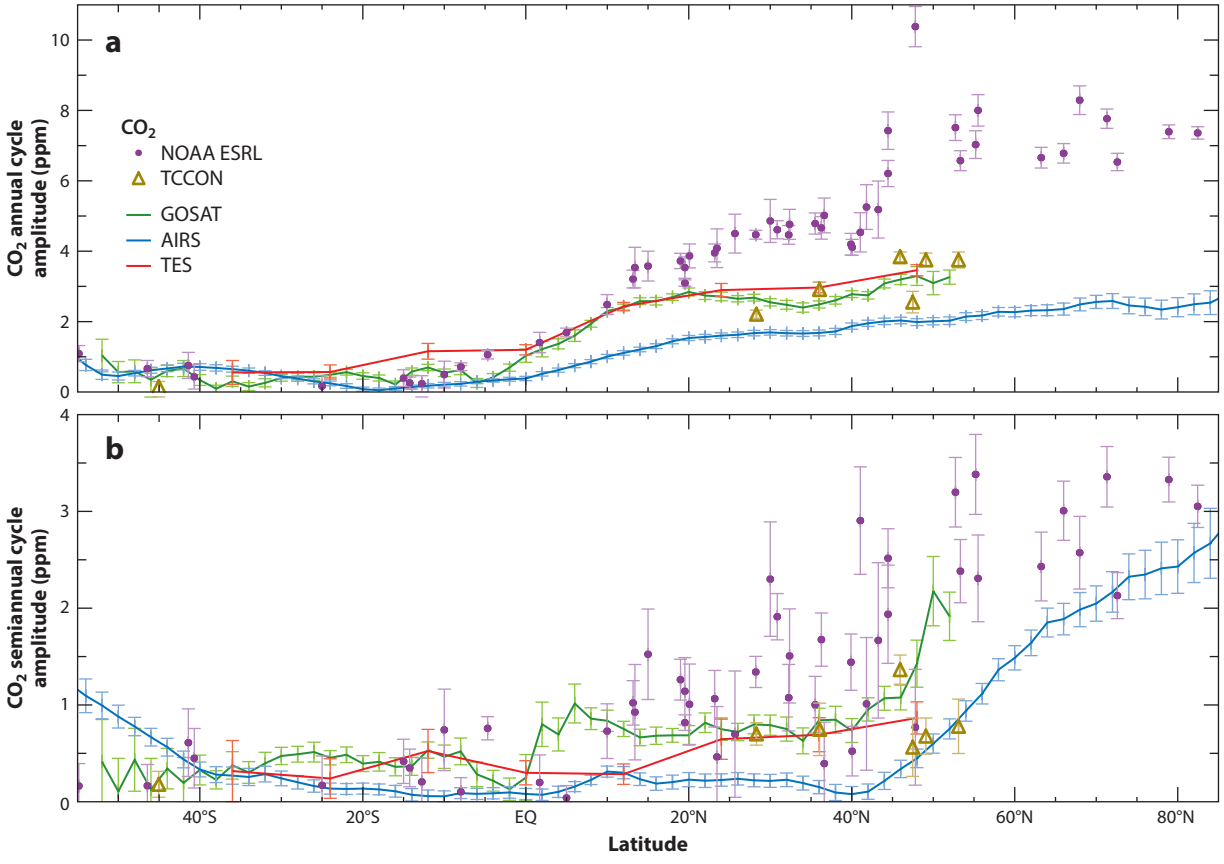

Figure 3

Latitudinal distributions of (*a*) CO_2 annual cycle amplitudes and (*b*) CO_2 semiannual cycle amplitudes. Shown are results from AIRS mid-tropospheric CO_2 (*blue lines*), GOSAT X_{CO2} (*green lines*), TES mid-tropospheric CO_2 (*red lines*), NOAA ESRL surface CO_2 (*purple dots*), and TCCON X_{CO2} (*dark yellow triangles*). Abbreviations: AIRS, Atmospheric Infrared Sounder; CO_2, carbon dioxide; GOSAT, Greenhouse gases Observing SATellite; NOAA ESRL, National Oceanic and Atmospheric Administration Earth System Research Laboratory; TCCON, Total Carbon Column Observing Network; TES, Tropospheric Emission Spectrometer. Figure adapted with permission from Jiang et al. (2016).

duration of each phase is 6 days. The positive rainfall anomalies are associated with enhanced rising air, which will bring more CO_2 from the surface to the mid-troposphere, as shown in **Figure 4**. The sinking air can bring low concentrations of CO_2 from high altitudes to the mid-troposphere, contributing to negative CO_2 anomalies. These MJO-related CO_2 anomalies propagate from west to east as shown in phases 1–8 in **Figure 4**. The peak-to-peak CO_2 amplitude of the composite MJO modulation is about 1 ppm.

MJO can also modulate CO_2 concentrations in the high latitudes. Li (2018) explored AIRS mid-tropospheric CO_2 over the Arctic region. MJO was separated into four different phases (phase 8 + 1, phase 2 + 3, phase 4 + 5, and phase 6 + 7). As shown in **Figure 5**, Arctic CO_2 anomalies are negative during phase 8 + 1 and positive during phase 4 + 5. The amplitude of MJO-related Arctic CO_2 anomalies is about 1.2 ppm. The Arctic MJO–related CO_2 anomalies represent a teleconnection between MJO and the polar atmosphere (Li 2018). The mechanism by which MJO influences CO_2 in the Arctic needs to be investigated in the future (Li 2018).

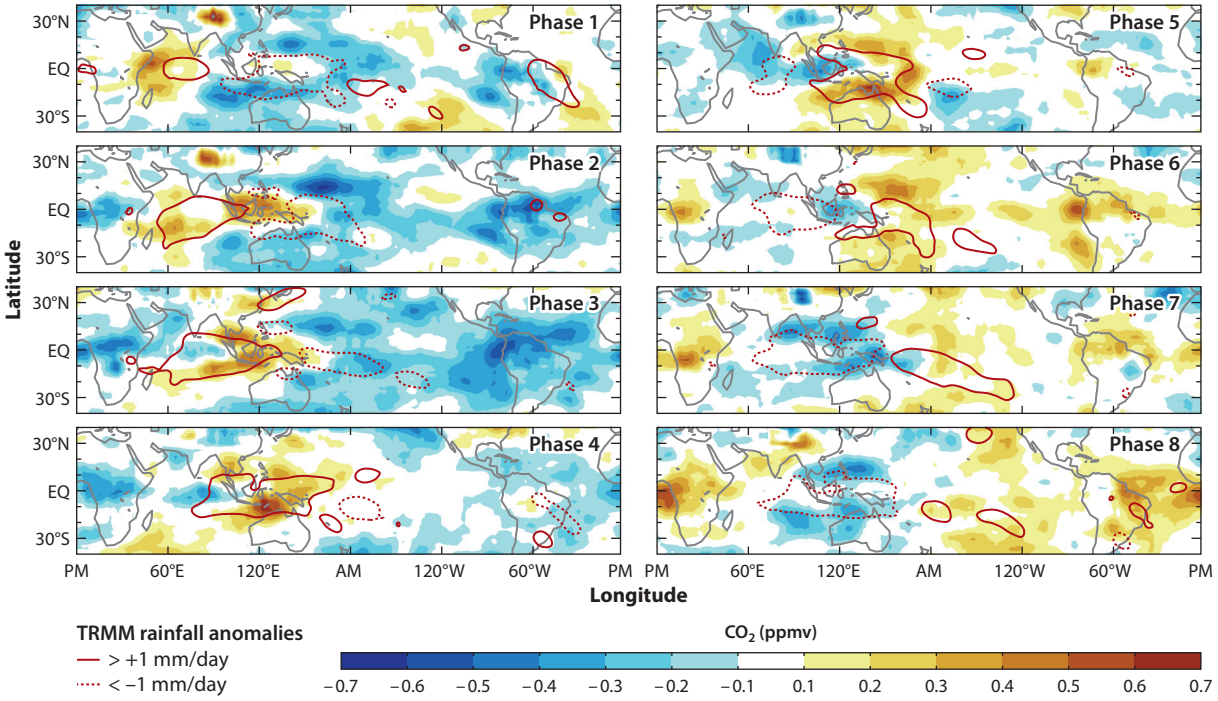

Figure 4

MJO-related AIRS CO_2 anomalies (*color*) and MJO-related rainfall anomalies (*contours*) for eight MJO phases. Abbreviations: AIRS, Atmospheric Infrared Sounder; CO_2, carbon dioxide; MJO, Madden-Julian Oscillation; TRMM, Tropical Rainfall Measuring Mission. Figure adapted with permission from Li et al. (2010).

2.2.2. Influence of stratospheric sudden warming. In addition to the MJO signal in mid-tropospheric CO_2, stratospheric sudden warming (SSW) can also modulate CO_2 concentrations. SSW is an important source of variability in the polar stratosphere. During SSW, the polar stratospheric temperature increases and the circumpolar wind reverses direction in a few days (Jiang et al. 2013b). The stratospheric polar vortex weakens, the positive temperature anomalies propagate downward, and there is less sinking air in the polar region during SSW (Limpasuvan et al. 2004). SSW can influence tracer concentrations (e.g., Manney et al. 2009, Sofieva et al. 2012, Jiang et al. 2013b). Jiang et al. (2013b) investigated the influence of SSW on the mid-tropospheric CO_2 retrievals from AIRS. AIRS mid-tropospheric CO_2 concentrations were explored before (**Figure 6*a*,*c***) and after (**Figure 6*b*,*d***) SSW events. It was found that mid-tropospheric CO_2 concentrations increased by 2–3 ppm within a few days after SSW events. After the SSW, the polar vortex areas shrank. In the horizontal direction, strong northward winds can bring mid-latitude, high-concentration CO_2 into the polar region (**Figure 6*b*,*d***). In the vertical direction, the reduced sinking air leads to less stratosphere-troposphere exchange, which can contribute to the CO_2 increase after the SSW (Jiang et al. 2013b). It is still a challenge to simulate the influence of SSW on model CO_2 (Jiang et al. 2013b).

2.3. Interannual Variability of CO_2

In addition to the annual cycle, semiannual cycle, and intraseasonal variability, atmospheric CO_2 also demonstrates interannual variability.

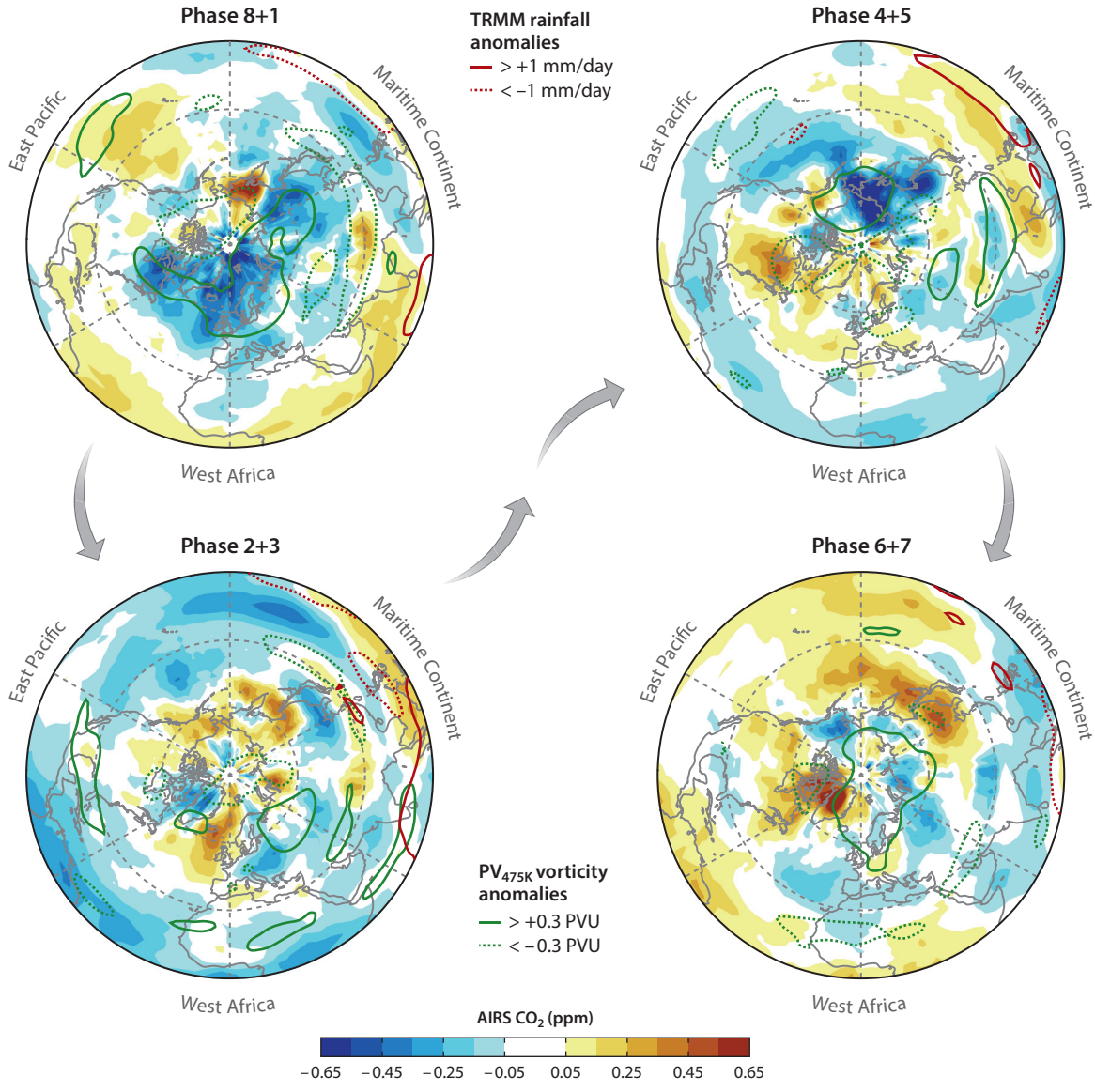

Figure 5

MJO-related AIRS CO_2 anomalies (*color*), MJO-related rainfall anomalies (*dark red contours*), and isentropic potential vorticity anomalies (*dark green contours*). Abbreviations: AIRS, Atmospheric Infrared Sounder; CO_2, carbon dioxide; MJO, Madden-Julian Oscillation; PVU, potential vorticity unit, TRMM, Tropical Rainfall Measuring Mission. Figure adapted with permission from Li (2018).

2.3.1. Influence of the El Niño-Southern Oscillation. In the tropical region, the El Niño–Southern Oscillation (ENSO) is the most important source of interannual variability. During ENSO events, sea surface temperature is high over the central and eastern Pacific, and convection and rain form over the central Pacific (Gage & Reid 1987). Previous studies (Bacastow 1976, Bacastow et al. 1980) suggested that the surface CO_2 concentrations could be modulated by ENSO. It was also noticed that the rate of atmospheric CO_2 rise increases at the surface

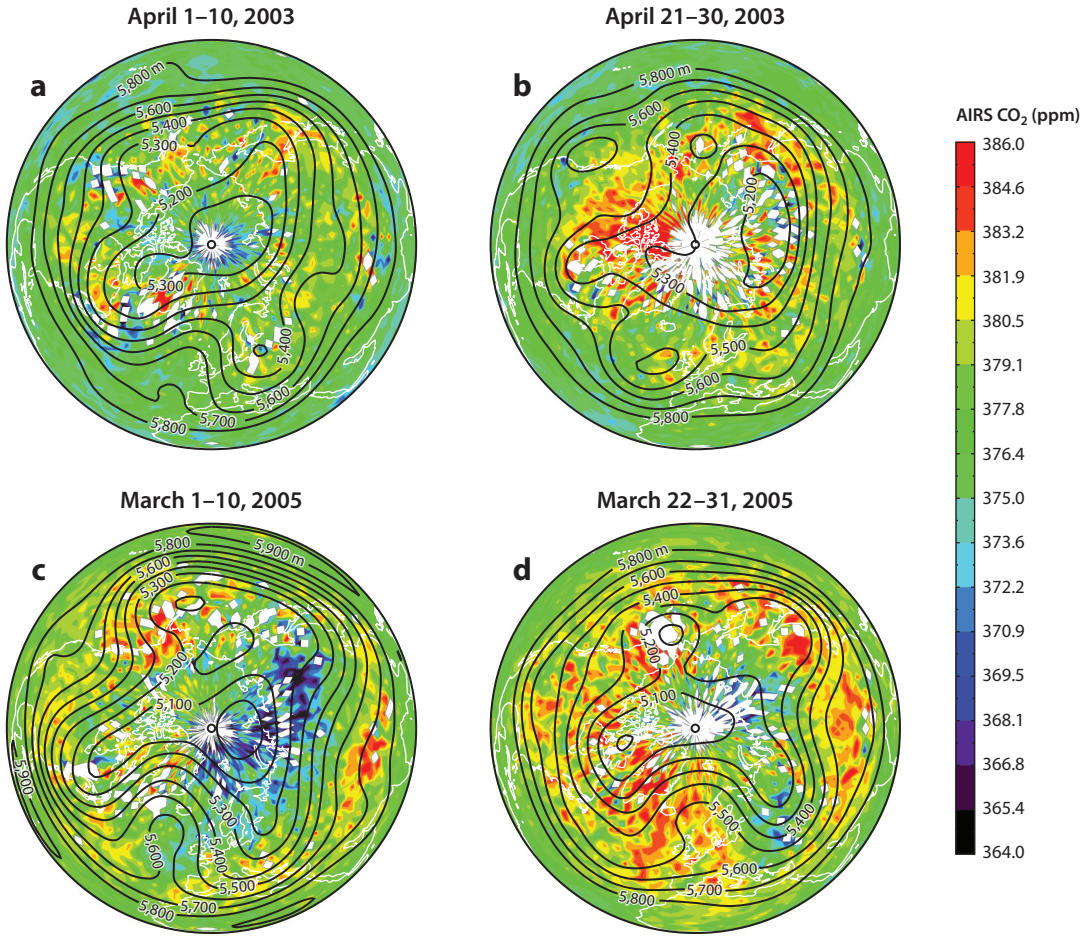

Figure 6

AIRS CO_2 data averaged in (*a*) April 1–10, 2003, and (*c*) March 1–10, 2005 (before SSW events), and (*b*) April 21–30, 2003, and (*d*) March 22–31, 2005 (after SSW events). Units for AIRS CO_2 are in parts per million. Black contours are NCEP2 500-hPa geopotential height data averaged over the same time periods as AIRS CO_2. Abbreviations: AIRS, Atmospheric Infrared Sounder; CO_2, carbon dioxide; NCEP2, National Centers for Environmental Prediction 2; SSW, stratospheric sudden warming. Figure adapted from Jiang et al. (2013b); copyright the American Meteorological Society.

during ENSO events (Keeling et al. 1995, Jones et al. 2001). During ENSO events, the upwelling of ocean water ceases at the South American coast, which decreases the CO_2 concentration in surface water (Feely 1987; Inoue & Sugimura 1992; Wong et al. 1993; Feely et al. 1997, 2006). However, the terrestrial biosphere becomes a larger source of atmospheric CO_2 due to the increase of respiration during ENSO events (Francey et al. 1995, Keeling et al. 1995, Jones et al. 2001). The net effect from land and ocean is that the surface CO_2 growth rate increases during ENSO events. These previous studies mainly focus on a few surface stations.

Satellite CO_2 retrievals confirm that ENSO can modulate mid-tropospheric CO_2 concentration. During ENSO, air rises over the central Pacific, which will bring high-concentration surface CO_2 to the mid-troposphere. Air sinks over the western Pacific, which will bring low-concentration CO_2 from high altitudes to the mid-troposphere. As a result, there is more AIRS mid-tropospheric CO_2 over the central Pacific (where air is ascending) and less AIRS

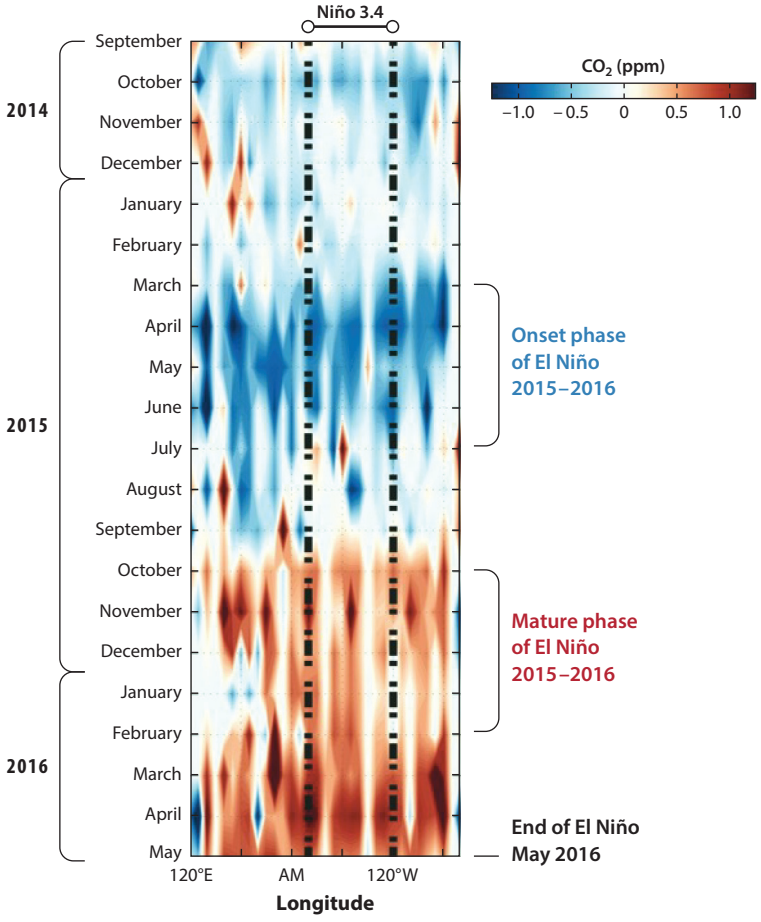

Figure 7

Time evolution of OCO-2 detrended X_{CO2} anomalies averaged over 5°S to 5°N. Abbreviation: CO_2, carbon dioxide; OCO-2, Orbiting Carbon Observatory 2. Figure adapted from Chatterjee et al. (2017) with permission from AAAS.

mid-tropospheric CO_2 over the western Pacific (where air is descending) during ENSO events (Jiang et al. 2010, Jiang et al. 2013a). Similar results are also seen in MOZART-2 mid-tropospheric CO_2 data; however, the ENSO signal is weaker in the model than in those from AIRS mid-tropospheric observations (Jiang et al. 2013a). Using OCO-2 column CO_2, Chatterjee et al. (2017) found a strong correlation between atmospheric CO_2 and ENSO. As shown in **Figure 7**, there is a negative X_{CO2} anomaly during the onset phase of ENSO, which is related to the decreased upwelling in the tropical Pacific Ocean (Chatterjee et al. 2017). Positive X_{CO2} anomalies are seen during the mature and end phase of ENSO, which is due to the terrestrial component of the carbon cycle, especially the enhanced fire emissions (Chatterjee et al. 2017). It was also found that the biosphere released more CO_2 into the atmosphere during the 2015–2016 ENSO compared to normal years (Liu et al. 2017).

2.3.2. Influence of the Tropospheric Biennial Oscillation. The Tropospheric Biennial Oscillation (TBO) is another important source of interannual variability in the tropical region. TBO

is defined as an oscillation in the strength of the Asian monsoon. The Asian monsoon may be strong in one year and weak in another year within a period of two years (Mooley & Parthasarathy 1984). During a strong monsoon year, the strong western Walker circulation is associated with strong rising air over the Indo-Pacific (Chang & Li 2000), which can bring more CO_2 from the surface to the mid-troposphere (Wang et al. 2011). AIRS mid-tropospheric CO_2 data averaged over strong and weak monsoon years are shown in **Figure 8*a,b***, respectively. The difference and corresponding significance level are shown in **Figure 8*c,d***, respectively. Mid-tropospheric CO_2 concentrations are higher over the Indo-Pacific Ocean during strong monsoon years, which are associated with strong rising air (Wang et al. 2011). The time series of AIRS mid-tropospheric CO_2 data averaged over the Indo-Pacific Ocean has a periodicity of around two years and correlates well with the TBO index. A similar TBO signal is also seen in model CO_2 concentrations from MOZART-2, although the magnitude of the TBO CO_2 signal in this model is weaker compared with those from AIRS mid-tropospheric CO_2 data (Wang et al. 2011).

2.3.3. Influence of annular modes. In high latitudes, annular modes are the most important source of interannual variability (Thompson & Wallace 1998). There are two annular modes: the Northern Annular Mode (NAM) and the Southern Annular Mode. The annular modes explain ~20–30% of the total variability of the geopotential height in the Northern and Southern Hemispheres and are characterized by opposite geopotential height anomalies in the polar region and mid-latitudes (Thompson & Wallace 2000). Jiang et al. (2010) found that the NAM can influence CO_2 concentration. Using mid-tropospheric data from AIRS, they explored the influence of the NAM on CO_2. As shown in **Figure 9*a***, the detrended polar CO_2 concentration correlates well with the detrended and inverted NAM index with a correlation coefficient of 0.7. AIRS mid-tropospheric CO_2 data averaged over strong polar vortex years (2005 and 2007) and weak polar vortex years (2006 and 2008) are shown in **Figure 9*b,c***, respectively. Overall, in high latitudes, there is less mid-tropospheric CO_2 in the polar region during strong polar vortex years than weak ones. When the polar vortex is strong, there is a strong jet stream, making it hard for CO_2 in mid-latitudes to penetrate into the polar region. During the strong polar vortex years, there is also increased photosynthetic uptake of atmospheric CO_2 in spring, which also contributes to negative CO_2 anomalies in the polar region (Russell & Wallace 2004, Schaefer et al. 2005, Jiang et al. 2010). The absolute amplitude of the CO_2 difference between the strong and weak polar vortex years is about 2–3 ppm, as shown in **Figure 9*d***. Similar results are expected for CO_2 over the Southern Hemisphere high latitudes when the data become available in the future.

3. OTHER SOURCES OF CO_2 VARIABILITY

3.1. Influence of Fire

Biomass burning is a major source for CO_2 in the atmosphere. Utilizing the latest X_{CO2} retrievals from OCO-2, Heymann et al. (2017) found that there was more atmospheric CO_2 during the fire season in 2015 at Indonesia than during normal seasons. OCO-2 X_{CO2}, background X_{CO2}, and X_{CO2} enhancements are shown in **Figure 10*a,b,c***, respectively. As shown in **Figure 10*c***, there was more atmospheric CO_2 during the fire event (about 2 ppm) (Heymann et al. 2017).

3.2. Influence of Volcanic Eruption

Volcanic eruptions also release CO_2 into the atmosphere. Schwandner (2017) explored a CO_2 release event from the Yasur volcano on Tanna Island, Vanuatu (19°S, 169°E), on May 30, 2015.

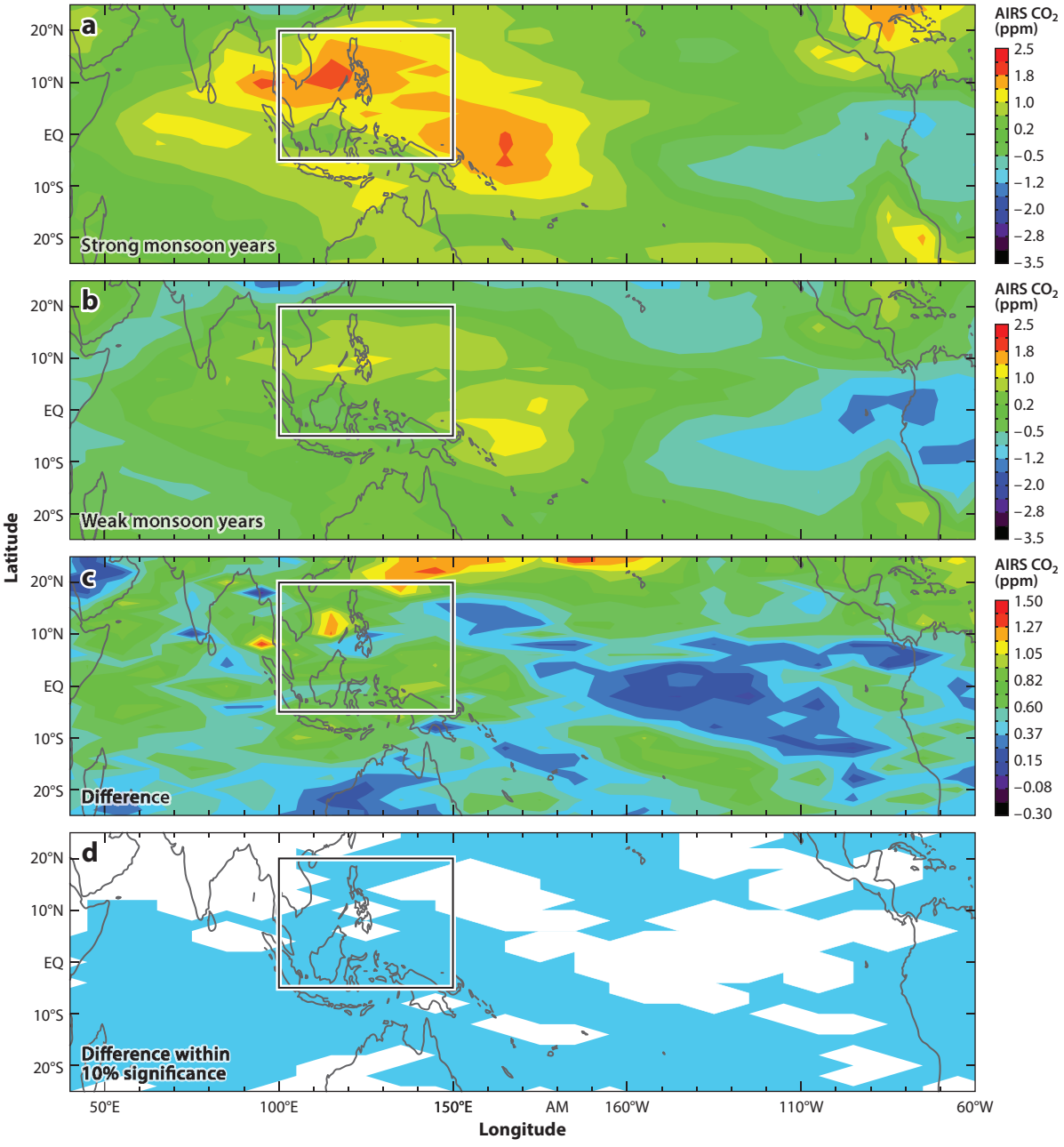

Figure 8

AIRS detrended mid-tropospheric CO_2 averaged over (*a*) strong monsoon years (JJAS of 2003, 2005, 2007, and 2010) and (*b*) weak monsoon years (JJAS of 2004, 2006, and 2008). (*c*) CO_2 differences between panels *a* and *b*. (*d*) CO_2 differences within 10% significance level (*blue*). The black rectangle highlights the Indo-Pacific region. Abbreviations: AIRS, Atmospheric Infrared Sounder; CO_2, carbon dioxide; JJAS, June, July, August, and September. Figure adapted with permission from Wang et al. (2011).

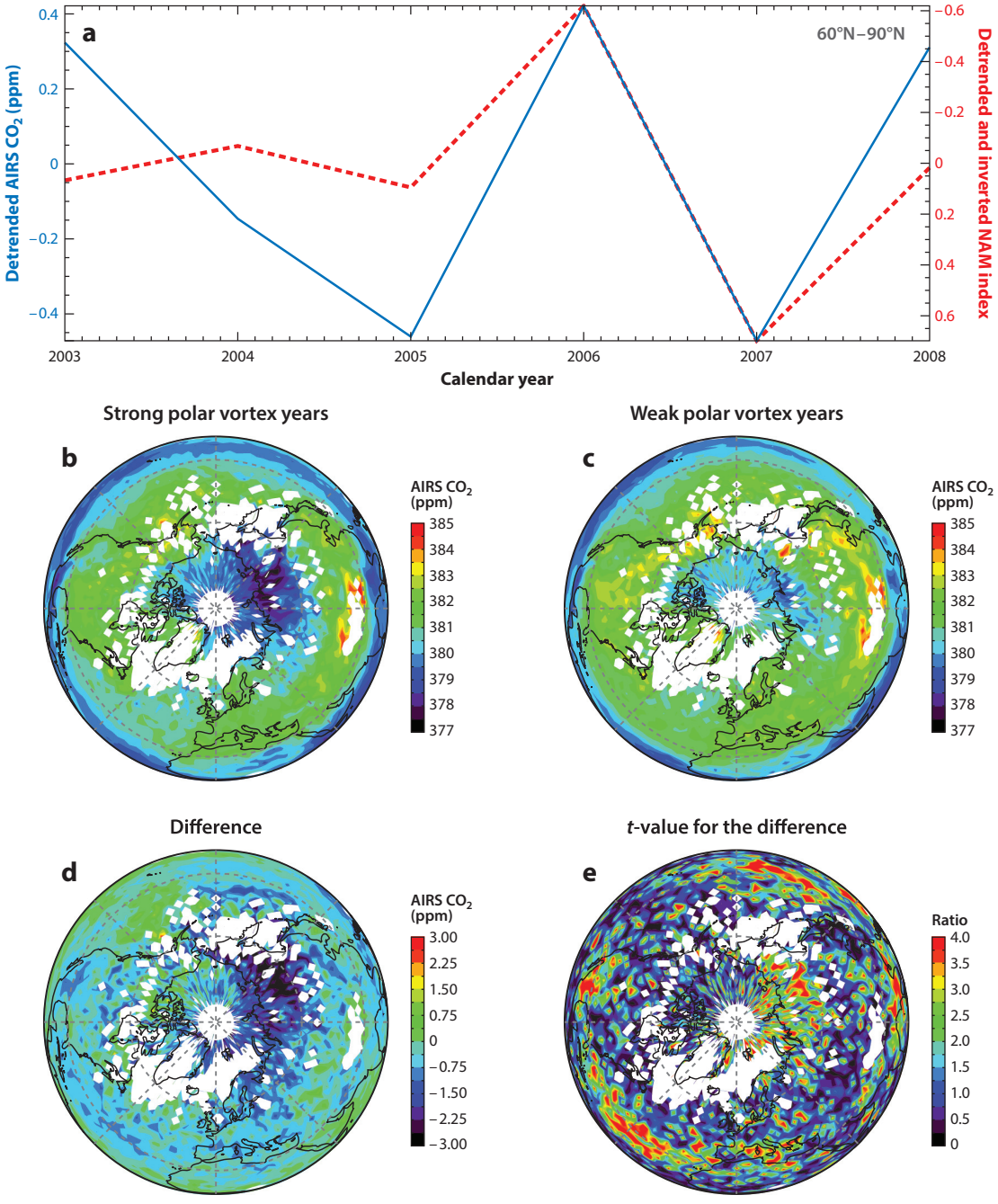

Figure 9

(*a*) AIRS detrended polar CO_2 (*blue solid line*) and detrended NAM index (*red dashed line*, *inverted*), (*b*) AIRS detrended CO_2 during strong polar vortex years (2005 and 2007), (*c*) AIRS detrended CO_2 during weak polar vortex years (2006 and 2008), (*d*) difference of AIRS CO_2 between strong and weak polar vortex years, and (*e*) *t*-value for the CO_2 difference. All CO_2 data are averaged from November to April. Abbreviations: AIRS, Atmospheric Infrared Sounder; CO_2, carbon dioxide; NAM, Northern Annular Mode. Figure adapted with permission from Jiang et al. (2010).

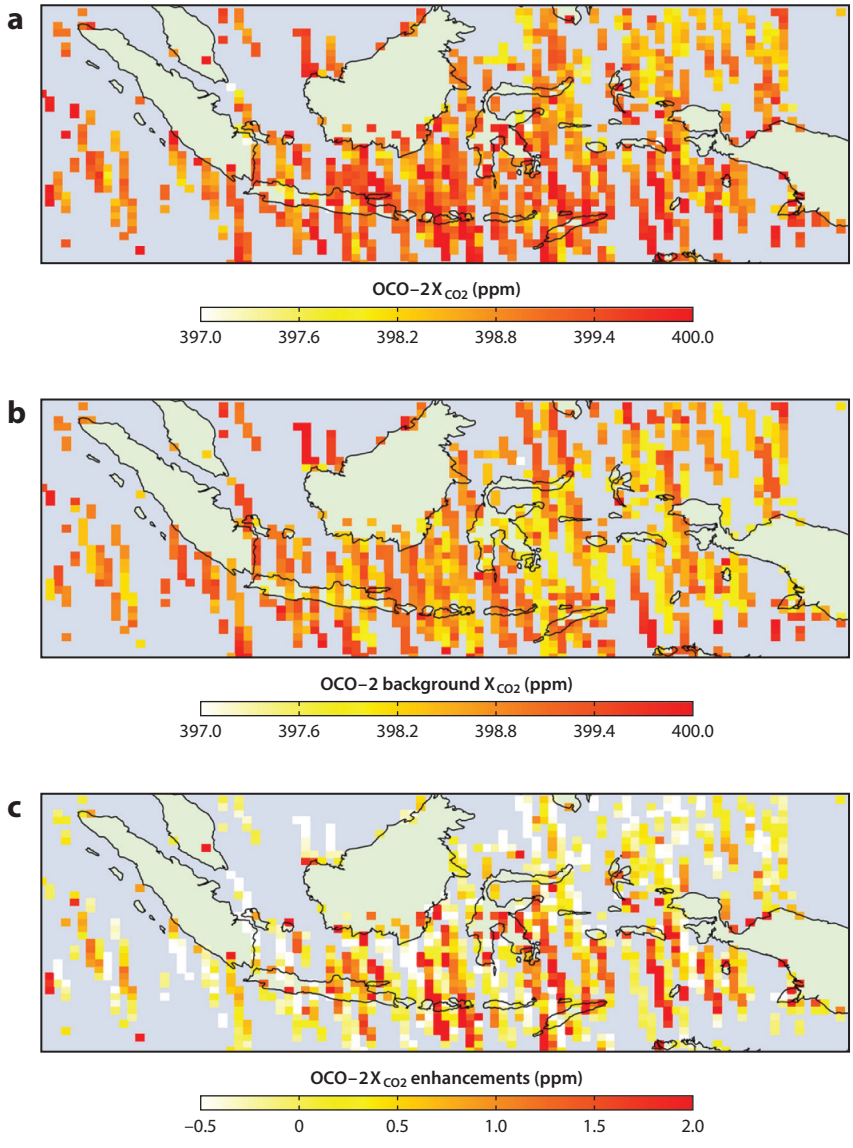

Figure 10

(*a*) OCO-2 X_{CO2} in July–November 2015, (*b*) background X_{CO2} in July–November 2015, and (*c*) X_{CO2} enhancements for the Indonesian region. Abbreviation: OCO-2, Orbiting Carbon Observatory 2. Figure adapted with permission from Heymann et al. (2017).

As shown in **Figure 11**, OCO-2 detected a high CO_2 plume from the volcano, and several high X_{CO2} footprints were found within 15 km downwind. A Gaussian plume model was used to simulate the enhancement of atmospheric CO_2 due to the eruption, and the model results were consistent with the X_{CO2} signal from OCO-2 (Schwandner 2017). The magnitude of the CO_2 enhancement due to the volcanic eruption was about 3.4 ppm near the crater vent (Schwandner 2017).

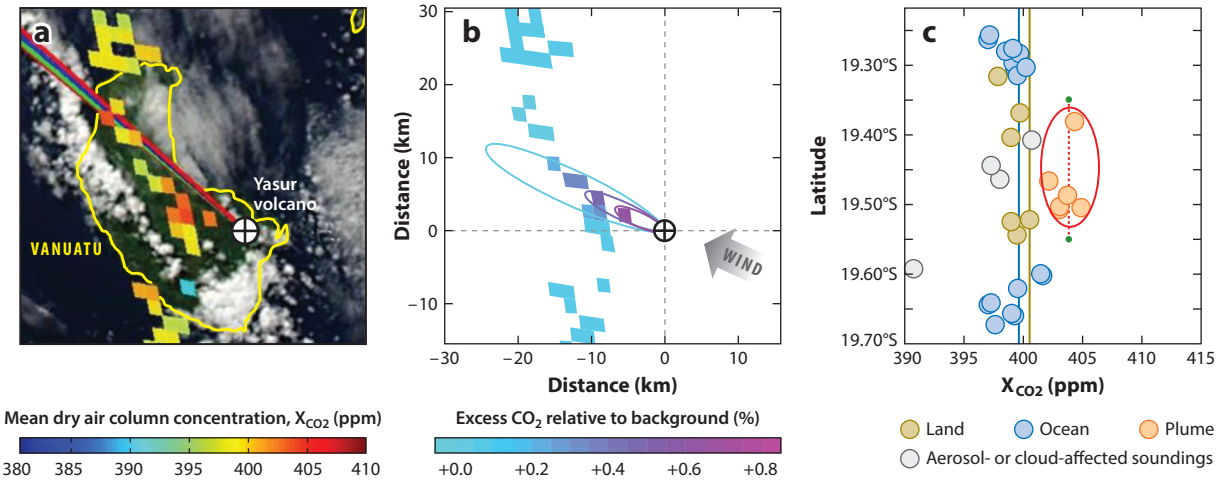

Figure 11

CO_2 plume emitted from the Yasur volcano in Vanuatu (*white circle with a black outline and cross*) on May 30, 2015. (*a*) OCO-2 X_{CO2} over MODIS composite imagery. (*b*) The order of magnitude of the X_{CO2} enhancement and the extent of the plume corresponding to a model CO_2 source of 41.6 kt/day at the time of overpass. (*c*) The magnitude of the excess shows X_{CO2} over ocean (*blue circles*), land (*brown circles*), and plume (*orange circles*). The red oval highlights the volcanic plume data (*orange circles*), and the red dashed line is the plume mean with the green end nodes representing the extent of the detectable plume. Abbreviations: CO_2, carbon dioxide; MODIS, Moderate Resolution Imaging Spectrometer; OCO-2, Orbiting Carbon Observatory 2. Figure adapted from Schwandner (2017) with permission from AAAS.

3.3. Influence of Drought

Atmospheric CO_2 concentrations can also be influenced by droughts, as demonstrated by Buermann et al. (2007) for the Mauna Loa record. Using satellite retrievals, Jiang et al. (2017) analyzed the impact of droughts on mid-tropospheric CO_2 over the southwestern United States. Mid-tropospheric CO_2 averaged over dry months [June, July, August, and September (JJAS) of 2003, 2007, and 2010] and wet months (JJAS of 2006, 2008, 2011, and 2012) are shown in **Figure 12*a*,*b***, respectively, and the difference between dry years and wet years and corresponding significance are shown in **Figure 12*c*,*d***, respectively. In this region, mid-tropospheric CO_2 concentrations in dry years are ~1 ppm higher than concentrations in wet years. Surface temperature is higher during droughts, which leads to an unstable environment and enhanced rising air. The increasing vertical motion can bring more CO_2 from the surface to upper levels. In addition, there is less CO_2 uptake from the biosphere due to reduced plant photosynthesis and greater soil respiration during droughts, which can contribute to the positive CO_2 anomaly during dry years (Jiang et al. 2017).

4. CONCLUSION

Recent satellite CO_2 data provide global distributions of CO_2, which offer a unique opportunity to explore CO_2 variability at different timescales (e.g., trend, intraseasonal, semiannual, annual, and interannual variability). Different satellite CO_2 retrievals (e.g., AIRS, ACE, IASI, GOSAT, OCO-2, and TES) capture the correct CO_2 seasonal cycle when compared with in situ CO_2 measurements. The CO_2 annual cycle has the largest amplitude at the surface, which decays with altitude. In addition to the annual cycle, atmospheric CO_2 concentration also demonstrates a semiannual cycle, which is related to the interaction between biosphere and atmosphere. Satellite

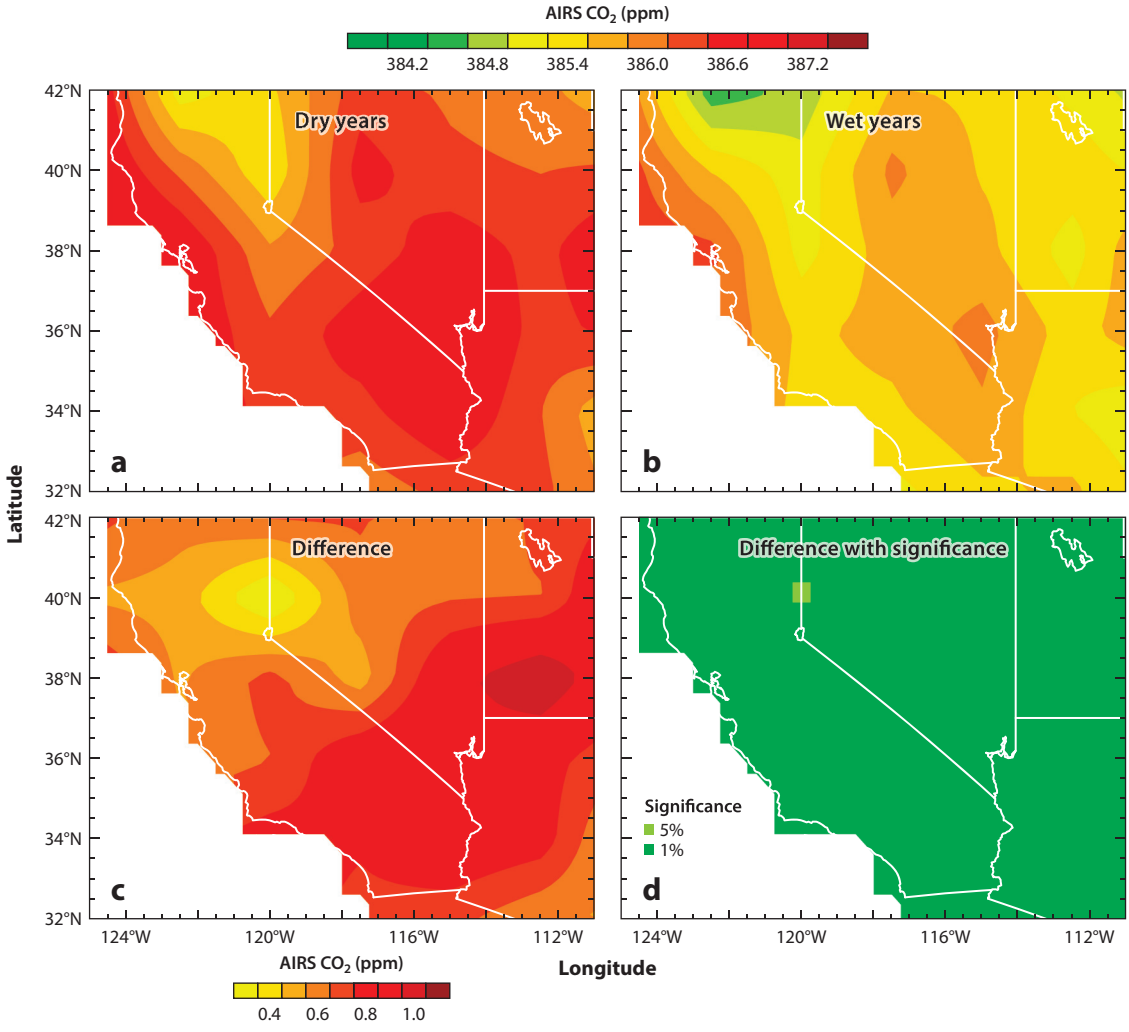

Figure 12

AIRS CO_2 concentrations averaged in (*a*) dry years (JJAS of 2003, 2007, and 2010) and (*b*) wet years (JJAS of 2006, 2008, 2011, and 2012), (*c*) CO_2 differences between panels *a* and *b*, and (*d*) CO_2 differences within 5% significance level (*light green*) and 1% significance level (*dark green*). Abbreviations: AIRS, Atmospheric Infrared Sounder; CO_2, carbon dioxide; JJAS, June, July, August, and September. Figure adapted with permission from Jiang et al. (2017).

CO_2 measurements can also be used to explore the intraseasonal variability of CO_2. The 30- to 90-day MJO oscillation can influence atmospheric CO_2 concentrations with a magnitude of 1 ppm at tropics and high latitudes. During an SSW event, CO_2 concentrations increase by 2–3 ppm within a few days. In addition to the semiannual cycle, annual cycle, and intraseasonal variability, atmospheric CO_2 also demonstrates variability at interannual timescales. ENSO, an important, large-scale component of interannual climate variability in the tropics, can modulate CO_2 concentrations with a magnitude of 1–2 ppm. TBO is related to the strengths of monsoon and western Walker circulation; it can modulate CO_2 concentrations over the Indo-Pacific region. At high latitudes, CO_2 concentrations can be influenced by the NAM. There is less CO_2 in the

polar region during the positive NAM years because of weak horizontal mixing and increased plant uptake of atmospheric CO_2 in spring. In addition to the intraseasonal and interannual variability, atmospheric CO_2 concentrations can also be modulated by fire, volcanic eruptions, and droughts. These results will help us better understand the natural variability of CO_2 and the interactions of atmospheric CO_2 with biosphere, biomass burning, and atmospheric circulation, which are critical for investigating the carbon budget.

Nearly half a century ago, a seminal paper by Lovelock (1971) argued for the usefulness of chlorofluorocarbons as indicators of atmospheric movements. Results summarized in this paper suggest that CO_2 has largely fulfilled Lovelock's vision for tracking atmospheric movement and circulation. It remains a challenge for atmospheric models to simulate the global patterns of variability of CO_2 summarized here. For example, preliminary modeling suggested that deep convection, which lofts CO_2 from the planetary boundary layer to the mid-troposphere, is underestimated in transport models (Jiang et al. 2008). Results from the variability of CO_2 can help us to identify possible deficiencies in the models and improve the models in the future.

DISCLOSURE STATEMENT

The authors are not aware of any affiliations, memberships, funding, or financial holdings that might be perceived as affecting the objectivity of this review.

ACKNOWLEDGMENTS

We thank the anonymous reviewer and Co-Editors for their time and helpful comments. We thank D. Crisp, A. Eldering, M. Gunson, C. Miller, E. Olsen, and T. Pagano for discussions and G. Chen, K.-F. Li, M.-C. Liang, V. Natraj, S. Newman, R.-L. Shia, Y. Wang, and Z.-C. Zeng for critical reading of the manuscript. We also thank K. Jucks for many years of support via the NASA OCO-2 project.

LITERATURE CITED

Bacastow RB. 1976. Modulation of atmospheric carbon dioxide by the Southern Oscillation. *Nature* 261:116–18

Bacastow RB, Adams J, Keeling CD, Moss D, Whorf T, Wong C. 1980. Atmospheric carbon dioxide, the southern oscillation, and the weak 1975 El Niño. *Science* 210:66–68

Bacastow RB, Keeling CD, Whorf TP. 1985. Seasonal amplitude increase in atmospheric CO_2 concentration at Mauna Loa, Hawaii, 1959–1982. *J. Geophys. Res.* 90(D6):10529–40

Barkley MP, Monks PS, Frieß U, Mittermeier RL, Fast H, et al. 2006. Comparisons between SCIAMACHY atmospheric CO_2 retrieved using (FSI) WFM-DOAS to ground based FTIR data and the TM3 chemistry transport model. *Atmos. Chem. Phys.* 6:4483–98

Boesch H, Baker D, Connor B, Crisp D, Miller C. 2011. Global characterization of CO_2 column retrievals from shortwave-infrared satellite observations of the Orbiting Carbon Observatory-2 mission. *Remote Sens.* 3:270–304

Buermann W, Lintner B, Koven C, Angert A, Pinzon JE, et al. 2007. The changing carbon cycle at the Mauna Loa Observatory. *PNAS* 104:4249–54

Chahine M, Barnet C, Olsen ET, Chen L, Maddy E. 2005. On the determination of atmospheric minor gases by the method of vanishing partial derivatives with application to CO_2. *Geophys. Res. Lett.* 32:L22803

Chahine M, Chen L, Dimotakis P, Jiang X, Li Q, et al. 2008. Satellite remote sounding of mid-tropospheric CO_2. *Geophys. Res. Lett.* 35:L17807

Chang CP, Li T. 2000. A theory for the tropical tropospheric biennial oscillation. *J. Atmos. Sci.* 57:2209–24

Chatterjee A, Gierach MM, Sutton AJ, Feely RA, Crisp D, et al. 2017. Influence of El Niño on atmospheric CO_2 over the tropical Pacific Ocean: findings from NASA's OCO-2 mission. *Science* 358:eaam5776

Choi Y, Vay SA, Vadrevu KP, Soja AJ, Woo J, et al. 2008. Characteristics of the atmospheric CO_2 signal as observed over the conterminous United States during INTEX-NA. *J. Geophys. Res.* 113(D7):D07301

Cleveland MS, Freeny AE, Graedel TE. 1983. The seasonal component of atmospheric CO_2: information from new approaches to the decomposition of seasonal time series. *J. Geophys. Res.* 88(C15):10934–46

Crevoisier C, Chédin A, Matsueda H, Machida T, Armante R, Scott NA. 2009. First year of upper tropospheric integrated content of CO_2 from IASI hyperspectral infrared observations. *Atmos. Chem. Phys.* 9:4797–810

Crisp D, Fisher BM, O'Dell C, Frankenberg C, Basilio R, et al. 2012. The ACOS CO_2 retrieval algorithm, part 2: global XCO_2 data characterization. *Atmos. Meas. Tech.* 5:687–707

Crisp D, Pollock HR, Rosenberg R, Chapsky L, Lee RAM, et al. 2017. The on-orbit performance of the Orbiting Carbon Observatory-2 (OCO-2) instrument and its radiometrically calibrated products. *Atmos. Meas. Tech.* 10:59–81

Dickinson RE, Cicerone RJ. 1986. Future global warming from atmospheric trace gases. *Nature* 319:109–15

Dupont F, Tanguay F, Li M, Perron G, Miller CM, et al. 2012. CARVE-FTS observations of Arctic CO_2, CH_4, and CO—overview of the instrument. *Proc. SPIE* 8532:853204

Eldering A, Wennberg PO, Crisp D, Schimel DS, Gunson MR, et al. 2017. The Orbiting Carbon Observatory-2 early science investigations of regional carbon dioxide fluxes. *Science* 358:eaam5745

Feely RA. 1987. Distribution of chemical tracers in the eastern equatorial Pacific during and after the 1982–1983 El Niño/Southern Oscillation event. *J. Geophys. Res.* 92(C6):6545–58

Feely RA, Takahashi T, Wanninkhof R, McPhaden MJ, Cosca CE, et al. 2006. Decadal variability of the air-sea CO_2 fluxes in the equatorial Pacific Ocean. *J. Geophys. Res.* 111(C8):C08S90

Feely RA, Wanninkhof R, Goyet C, Archer DE, Takahashi T. 1997. Variability of CO_2 distributions and sea-air fluxes in the central and eastern equatorial Pacific during the 1991–1994 El Niño. *Deep Sea Res. Part II Top. Stud. Oceanogr.* 44:1851–67

Fisher JB, Sikka M, Oechel WC, Huntzinger DN, Melton JR, et al. 2014. Carbon cycle uncertainty in the Alaskan Arctic. *Biogeosciences* 11:4271–88

Foucher PY, Chédin A, Armante R, Boone C, Crevoisier C, Bernath P. 2011. Carbon dioxide atmospheric vertical profiles retrieved from space observation using ACE-FTS solar occultation instrument. *Atmos. Chem. Phys.* 11:2455–70

Francey R, Tans PP, Allison CE, Enting IG, White JWC, Trolier M. 1995. Changes in oceanic and terrestrial carbon uptake since 1982. *Nature* 373:326–30

Gage KS, Reid GC. 1987. Longitudinal variations in tropical tropopause properties in relation to tropical convection and El Nino-Southern Oscillation events. *J. Geophys. Res.* 92(C13):14197–203

GLOBALVIEW-CO_2. 2010. *Cooperative Atmospheric Data Integration Project: Carbon Dioxide*. Boulder, CO: NOAA Environ. Sci. Res. Lab. CD-ROM

Goody RM, Yung YL. 1989. *Atmospheric Radiation: Theoretical Basis*. New York: Oxford Univ. Press

Heymann J, Reuter M, Buchwitz M, Schneising O, Bovensmann H, et al. 2017. CO_2 emission of Indonesian fires in 2015 estimated from satellite-derived atmospheric CO_2 concentrations. *Geophys. Res. Lett.* 44:1537–44

Inoue HY, Sugimura Y. 1992. Variations and distributions of CO_2 in and over the equatorial Pacific during the period from the 1986/88 El Niño event to the 1988/89 La Niña event. *Tellus Ser. B* 44:1–22

IPCC (Intergov. Panel Clim. Change). 2013. *Climate Change 2013: The Physical Science Basis: Contribution of Working Group I to the Fifth Assessment Report of the Intergovernmental Panel on Climate Change*, ed. TF Stocker, D Qin, GK Plattner, M Tignor, SK Allen, et al. Cambridge, UK/New York: Cambridge Univ. Press

Jiang X, Chahine MT, Li Q, Liang M, Olsen ET, et al. 2012. CO_2 semiannual oscillation in the middle troposphere and at the surface. *Glob. Biogeochem. Cycles* 26:GB3006

Jiang X, Chahine MT, Olsen ET, Chen LL, Yung YL. 2010. Interannual variability of mid-tropospheric CO_2 from Atmospheric Infrared Sounder. *Geophys. Res. Lett.* 37:L13801

Jiang X, Crisp D, Olsen ET, Kulawik SS, Miller CE, et al. 2016. CO_2 annual and semi-annual cycles from multiple satellite retrievals and models. *Earth Space Sci.* 3:78–87

Jiang X, Kao A, Corbett A, Olsen E, Pagano T, et al. 2017. Influence of droughts on mid-tropospheric CO_2. *Remote Sens.* 9:852

Jiang X, Li Q, Liang MC, Shia R, Chahine MT, et al. 2008. Simulation of upper tropospheric CO_2 from chemistry and transport models. *Glob. Biogeochem. Cycles* 22:GB4025

Jiang X, Waliser DE, Tian B, Li JL, Olsen WS, et al. 2009. Vertical heating structures associated with the MJO as characterized by TRMM estimates, ECMWF reanalyses, and forecasts: a case study during 1998/99 winter. *J. Climate* 22:6001–20

Jiang X, Wang J, Olsen ET, Liang M, Pagano TS, et al. 2013a. Influence of El Niño on mid-tropospheric CO_2 from Atmospheric Infared Sounder and model. *J. Atmos. Sci.* 70:223–30

Jiang X, Wang J, Olsen ET, Pagano T, Chen LL, Yung YL. 2013b. Influence of stratospheric sudden warming on AIRS mid-tropospheric CO_2. *J. Atmos. Sci.* 70:2566–73

Jones CD, Collins M, Cox PM, Spall SA. 2001. The carbon cycle response to ENSO: a coupled climate-carbon cycle model study. *J. Climate* 14:4113–29

Keeling CD, Chin JFS, Whorf TP. 1996. Increased activity of northern vegetation inferred from atmospheric CO_2 measurements. *Nature* 382:146–49

Keeling CD, Whorf TP, Wahlen M, Vanderplicht J. 1995. Interannual extremes in the rate of rise of atmospheric carbon dioxide since 1980. *Nature* 375:666–70

Knutson TR, Weickmann KM. 1987. 30–60 day atmospheric oscillations: composite life cycles of convection and circulation anomalies. *Mon. Weather Rev.* 115:1407–36

Kuang Z, Margolis J, Toon G, Crisp D, Yung YL. 2002. Spaceborne measurements of atmospheric CO_2 by high-resolution NIR spectrometry of reflected sunlight: an introductory study. *Geophys. Res. Lett.* 29:1716

Kulawik SS, Jones DBA, Nassar R, Irion FW, Worden JR, et al. 2010. Characterization of Tropospheric Emission Spectrometer (TES) CO_2 for carbon cycle science. *Atmos. Chem. Phys.* 10:5601–23

Kuze A, Suto H, Nakajima M, Hamazaki T. 2009. Thermal and near infrared sensor for carbon observation Fourier-transform spectrometer on the Greenhouse Gases Observing Satellite for greenhouse gases monitoring. *Appl. Opt.* 48:6716–33

Li KF. 2018. An intraseasonal variability in CO_2 over the Arctic induced by the Madden-Julian Oscillation. *Geophys. Res. Lett.* 45:1630–38

Li KF, Tian B, Waliser DE, Yung YL. 2010. Tropical mid-tropospheric CO_2 variability driven by the Madden-Julian Oscillation. *PNAS* 107:19171–75

Limpasuvan V, Thompson DWJ, Hartmann DL. 2004. The life cycle of the Northern Hemisphere sudden stratospheric warmings. *J. Climate* 17:2584–96

Lindqvist H, O'Dell CW, Basu S, Boesch H, Chevallier F, et al. 2015. Does GOSAT capture the true seasonal cycle of carbon dioxide? *Atmos. Chem. Phys.* 15:13023–40

Liu J, Bowman KW, Schimel DS, Parazoo NC, Jiang Z, et al. 2017. Contrasting carbon cycle responses of the tropical continents to the 2015–2016 El Niño. *Science* 358:eaam5690

Lovelock JE. 1971. Atmospheric fluorine compounds as indicators of air movements. *Nature* 230:379

Madden RA, Julian PR. 1971. Detection of a 40–50 day oscillation in zonal wind in tropical Pacific. *J. Atmos. Sci.* 28:702–8

Manney GL, Schwartz MJ, Kruger K, Santee ML, Pawson S, et al. 2009. Aura Microwave Limb Sounder observations of dynamics and transport during the record-breaking 2009 Arctic stratospheric major warming. *Geophys. Res. Lett.* 36:L12815

Matsueda H, Inoue HY, Ishii M. 2002. Aircraft observation of carbon dioxide at 8–13 km altitude over the western Pacific from 1993 to 1999. *Tellus Ser. B* 54:1–21

Mooley DA, Parthasarathy B. 1984. Fluctuations in All-India summer monsoon rainfall during 1871–1978. *Clim. Change* 6:287–301

Nguyen H, Osterman G, Wunch D, O'Dell C, Mandrake L, et al. 2014. A method for collocating satellite X_{CO_2} data to ground-based data and its application to ACOS-GOSAT and TCCON. *Atmos. Meas. Tech.* 7:2631–44

Pearman GI, Hyson P. 1980. Activities of the global biosphere as reflected in atmospheric CO_2 records. *J. Geophys. Res.* 85(C8):4457–67

Pearman GI, Hyson P. 1981. The annual variation of atmospheric CO_2 concentration observed in the northern hemisphere. *J. Geophys. Res.* 86(C10):9839–43

Petzold A, Thouret V, Gerbig C, Zahn A, Brenninkmeijer CAM, et al. 2015. Global-scale atmosphere monitoring by in-service aircraft—current achievements and future prospects of the European Research Infrastructure IAGOS. *Tellus Ser. B* 67:28452

Rinsland CP, Chiou LS, Boone C, Bernath P. 2010. Carbon dioxide retrievals from Atmospheric Chemistry Experiment solar occultation measurements. *J. Geophys. Res.* 115(D3):D03105

Russell JL, Wallace JM. 2004. Annual carbon dioxide drawdown and the Northern Annular Mode. *Glob. Biogeochem. Cycles* 18:GB1012

Sarmiento JL, Wofsy S. 1999. *A U.S. Carbon Cycle Science Plan: A Report of the Carbon and Climate Working Group*. Washington, DC: US Glob. Change Res. Program

Schaefer K, Denning S, Leonard O. 2005. The winter Arctic Oscillation, the timing of spring, and carbon fluxes in the Northern Hemisphere. *Glob. Biogeochem. Cycles* 19:GB3017

Schwandner F. 2017. Spaceborne detection of localized carbon dioxide sources. *Science* 358:eaam5782

Shia R, Liang M, Miller CE, Yung Y. 2006. CO_2 in the upper troposphere: influence of stratosphere-troposphere exchange. *Geophys. Res. Lett.* 33:L14814

Shiomi K, Kawakami S, Kina T, Mitomi Y, Yoshida M, et al. 2008. GOSAT Level 1 processing and in-orbit calibration plan. *Proc. SPIE* 7106:71060O

Singh H, Jacob D, Pfister L. 2002. *INTEX-NA: Intercontinental Chemical Transport Experiment—North America*. White Pap., NASA Ames Res. Cent., Moffett Field, CA. **https://geo.arc.nasa.gov/sgg/singh/white_paper.pdf**

Sofieva VF, Kalakoski N, Verronen PT, Paivarinta SM, Kyrola E, et al. 2012. Polar-night O_3, NO_2 and NO_3 distributions during sudden stratospheric warmings in 2003–2008 as seen by GOMOS/Envisat. *Atmos. Chem. Phys.* 12:1051–66

Strow L, Hannon S. 2008. A 4-year zonal climatology of lower-tropospheric CO_2 derived from ocean-only Atmospheric Infrared Sounder observations. *J. Geophys. Res.* 113(D18):D18302

Tans P, Bakwin PS, Bruhwiler L, Conway TJ, Dlugokencky EJ, et al. 1998. Carbon cycle. In *Climate Monitoring and Diagnostics Laboratory: Summary Report No. 24 1996–1997*, ed. DJ Hoffmann, JT Peterson, RM Rosson, Clim. Monit. Diagn. Lab., pp. 30–51. Boulder, CO: Natl. Ocean. Atmos. Admin. Environ. Res. Lab.

Tans P, Keeling R. 2014. *Trends in atmospheric carbon dioxide*. Rep., Natl. Ocean. Atmos. Adm. Earth Syst. Res. Lab., Washington, DC. **https://www.esrl.noaa.gov/gmd/ccgg/trends/**

Thompson DWJ, Wallace JM. 1998. The Arctic Oscillation signature in the wintertime geopotential height and temperature fields. *Geophys. Res. Lett.* 25:1297–300

Thompson DWJ, Wallace JM. 2000. Annular modes in the extratropical circulation. Part I: month-to-month variability. *J. Climate* 13:1000–16

Tian BJ, Yung YL, Waliser DE, Tyranowski T, Kuai L, et al. 2007. Intraseasonal variations of the tropical total ozone and their connection to the Madden-Julian Oscillation. *Geophys. Res. Lett.* 34:L08704

Wang J, Jiang X, Chahine MT, Liang M, Olsen MT, et al. 2011. The influence of tropospheric biennial oscillation on mid-tropospheric CO_2. *Geophys. Res. Lett.* 38:L20805

Washenfelder RA, Toon GC, Blavier JF, Yang Z, Allen NT, et al. 2006. Carbon dioxide column abundances at the Wisconsin Tall Tower site. *J. Geophys. Res.* 111(D22):D22305

Watanabe H, Ishihara H, Hayashi K, Kawazoe F, Kikuchi N, et al. 2008. Detailed design of the GOSAT DHF at NIES and data acquisition/processing/distribution strategy. *Proc. SPIE* 7106:71060N

Wofsy SC. 2011. HIAPER Pole-to-Pole Observations (HIPPO): fine-grained, global-scale measurements of climatically important atmospheric gases and aerosols. *Philos. Trans. R. Soc. A* 369:2073–86

Wong CS, Chan YH, Page JS, Smith GE, Bellegay RD. 1993. Changes in equatorial CO_2 flux and new production estimated from CO_2 and nutrient levels in Pacific surface waters during the 1986/87 El Niño. *Tellus Ser. B* 45:64–79

Wunch D, Wennberg PO, Toon GC, Connor BJ, Fisher B, et al. 2011. A method for evaluating bias in global measurement of CO_2 total columns from space. *Atmos. Chem. Phys.* 11:12317–37

Yang Z, Washenfelder RA, Keppel-Aleks G, Wennberg PO, Krakauer NY, et al. 2007. New constraints on Northern Hemisphere growing season net flux. *Geophys. Res. Lett.* 34:L12807

Yokota T, Yoshida Y, Eguchi N, Ota Y, Tanaka T, et al. 2009. Global concentrations of CO_2 and CH_4 retrieved from GOSAT: first preliminary results. *SOLA* 5:160–63

Annual Review
of Earth and
Planetary Sciences
Volume 47, 2019

Contents

Errata

An online log of corrections to *Annual Review of Earth and Planetary Sciences* articles may be found at http://www.annualreviews.org/errata/earth